

# A two-parameter, minimal-data model to predict dengue cases: the 2022–2023 outbreak in Florida, USA

Saman Hosseini<sup>1\*</sup>, Lee W. Cohnstaedt<sup>2</sup>, Caterina Scoglio<sup>1</sup>

**1** Department of Electrical and Computer Engineering, Kansas State University, Manhattan, KS, USA

**2** Foreign Arthropod-Borne Animal Diseases Research Unit National Bio- and Agro-defense Facility, USDA ARS , Manhattan, KS, USA

\* Shosseini@ksu.edu

## Abstract

Reliable and timely dengue predictions provide actionable lead time for targeted vector control and clinical preparedness, reducing preventable diseases and health-system costs in at-risk communities. Dengue forecasting often relies on site-specific covariates and entomological data, limiting generalizability in data-sparse settings. We propose a data-parsimonious (DP) framework based on the incidence versus cumulative cases (ICC) curve, extending it from a basic SIR to a two-population SEIR model for dengue. Our DP model uses only the target season’s incidence time series and estimates only two parameters, reducing noise and computational burden. A Bayesian extension quantifies the case reporting and fitting uncertainty to produce calibrated predictive intervals. We evaluated the performance of the DP model in the 2022-2023 outbreaks in Florida, where standardized clinical tests and reporting support accurate case determination. The DP framework demonstrates competitive predictive performance at substantially lower computational cost than more elaborate models, making it suitable for dengue early detection where dense surveillance or long historical records are unavailable.

## Author summary

Dengue is a mosquito-borne viral disease that is expanding into new regions and affecting public health systems. To act early, local officials need reliable short-term forecasts of dengue cases, but many existing models depend on detailed mosquito, climate, or long-term historical data that are often unavailable. We present a simple dengue forecasting framework that uses only one input: the weekly number of reported human cases in the current season. The method is advanced from the incidence versus cumulative cases (ICC) curves for basic SIR to the two-population SEIR model of dengue. A Bayesian extension quantifies the uncertainty from both imperfect reporting and model fitting, providing Bayesian prediction densities instead of single best guesses. We applied this framework to the 2022–2023 dengue outbreaks in Florida, where standardized laboratory tests support accurate case reporting. Despite its minimal data requirements and low computational cost, the model achieves competitive predictive performance. This makes it a practical option for dengue early detection in settings with limited entomological surveillance or incomplete historical records.

# 1 Introduction

Dengue is the most prevalent arthropod-borne viral infection in the human population [1, 2], transmitted by mosquitoes of the genus *Aedes* [3]. It comprises four antigenically distinct serotypes (DENV-1, DENV-2, DENV-3 and DENV-4). It places roughly half of the world’s population at risk and causes an estimated 100–400 million infections each year [4]. Transmission occurs in tropical and subtropical regions, particularly in urban and peri-urban settings. Most infections are asymptomatic or mild, but a proportion progresses to severe disease that can be fatal [5].

Although dengue vaccines are available, there is no proven, specific antiviral therapy for dengue [6]. In addition, the performance of the vaccine has important limitations: its effectiveness varies by serotype, usually stronger for DENV-1 / 2 and weaker or uncertain for DENV-3 / 4, and its protection is generally higher in previously exposed individuals (seropositive) than in seronegative recipients [7]. Given the limitations of dengue vaccination, population-level measures, such as vector control programs and public health alerts, remain essential to reduce transmission [8, 9]. Consequently, accurate forecasting is integral to effective mitigation. Accurate forecasts enable vector control agencies to reduce transmission risk by reducing mosquito populations through larviciding and adulticiding, deploying biotechnological approaches (e.g., sterile insect technique) [10], or combining these strategies, while timely public health advisories increase the community’s uptake of personal protective measures. Thus, reliable forecasting moves mitigation from reaction to prevention, enhancing cost efficiency and health outcomes.

To operationalize such forecasting, models rely on measurable drivers drawn from multiple data streams. There are various data sources to predict the risk of dengue transmission to humans. A strong correlation between dengue incidence and *Aedes* spp. abundance has been shown [11–13]; thus, a large number of models incorporate entomological drivers to predict the risk of transmission from the mosquito to the human population. Consequently, due to the correlation between mosquito abundance and climatological variables such as temperature, rainfall, and humidity [14–17] climatological drivers are also widely used in dengue forecasting models. In general, the data used for the models can be classified as direct and indirect factors [18]. Direct factors are those that immediately act on vector biology and dengue transmission by altering the mosquito life cycle or virus dynamics; they include climate and weather drivers (rainfall, temperature, humidity, drought, El Niño) [19–29], mosquito density measures (positive containers in houses inspected; larval, pupal, and adult counts) [30–36], dengue virus serotypes, vertical transmission [23, 37], and human biting rate [38, 39]. Indirect factors are contextual conditions that shape outbreaks without directly changing larval counts: geography and topography [40, 41] and urban–rural setting [42, 43]; spatial and spatiotemporal patterns [44–46]; population movement and trade [47–53]; environmental, land-use, and sanitation conditions; and host immunology and the vaccination landscape.

The combination of direct and indirect factors has been used to establish predictive frameworks to forecast risk at different locations. Hii et al. (2012) built a weather-based dengue forecasting model for Singapore using Poisson regression with temperature and rainfall modeled as piecewise linear (spline) effects over long lag windows, plus AR lags, trend, seasonality, and a population offset [54]. Descloux et al. (2012) developed a support vector machine (SVM) model for dengue outbreak forecasts for Noumea (New Caledonia) using epidemiological surveillance data, local meteorological variables, and large-scale climate indices [55]. Lowe et al. (2014) used a Bayesian negative binomial GLMM for monthly dengue forecast in Brazil with fixed effects for 3-month temperature and precipitation anomalies, altitude, population density, and 4-month lagged dengue risk, plus seasonal random effects and zones varying [56]. Shi et al. (2016) trained 12

horizon-specific LASSO models [57] to predict Singapore’s weekly dengue 1–12 weeks ahead using recent case counts, vector breeding indices, meteorological variables and population statistics [58]. Lowe et al. (2016) developed a Bayesian negative binomial spatiotemporal GLMM for Brazil, driven by seasonal climate forecasts (3-month temperature/precipitation anomalies), population density, altitude and a 4 month lagged dengue signal, with spatial effects and zone-varying seasonality; generated 3–4 month probabilistic risk maps of 3–4 months that outperformed a seasonal baseline [59]. Alkhateeb et al. (2018) described a probabilistic forecasting system, deployed in Brazil, Malaysia, and Mexico, that uses logistic regression in weekly surveillance, meteorological and entomological indicators to trigger alerts once the predicted outbreak probability exceeds a predefined threshold [60]. Additional models from various locations have used different drivers and methods for risk prediction [61–73].

These approaches have advanced operational forecasting in diverse settings; nevertheless, several limitations remain. Although many models perform well on timing, trajectory, and severity, they are often location-specific and fail to generalize to other settings. In particular, reliance on direct factors, such as entomological surveillance restricts use to sites where such data exist. Moreover, predictors that are strong at one site may be weak elsewhere; for example, humidity may be a primary driver in one location but show no correlation with outbreaks in another. In addition, in many settings, there are no accurate statistics on human cases, which means that case reporting is subject to substantial uncertainty for a variety of reasons. Beyond limited generalizability, two additional issues arise: parameter estimation adds noise and model selection is time-consuming and computationally intensive. Finally, many models are inapplicable for forecasting in locations without an outbreak history (newly infected locations).

To address these limitations, we developed and evaluated a DP framework based on the incidence versus cumulative cases (ICC) curve method. Lega (2016) introduced a parsimonious input data ICC model with a minimum number of parameters for a basic SIR model [74, 75]. In this work, we extended the ICC framework from a basic SIR to the SEIR model of dengue with two populations. The only two parameters of this model are estimated from human incidence data, reducing the noise of estimation. Moreover, because the only required input is the time series of new human cases in the target year, the approach is usable in data-limited settings without entomological surveillance and with minimal historical information. Finally, based on the theory of the ICC framework, we constructed a Bayesian predictive model that incorporates uncertainty in reported cases and in parameter estimation to enhance reliability and deliver narrower uncertainty intervals. We demonstrate its performance by forecasting dengue risk in Florida during 2022–2023. Our results show that the two-parameter ICC framework extended to the two-population SEIR model of dengue achieves competitive accuracy while requiring substantially less computation.

In Section 2, we describe the data, study location, the dengue compartmental model used to extend the ICC method, and the predictive framework, including point and Bayesian prediction and the metrics used to evaluate accuracy. Section 3 presents results separately for each outbreak, including the outbreak season, point and Bayesian predictions, and associated MCMC parameters. Section 4 discusses the results of the model.

## 2 Material and methods

In this section, we describe the data sources, study location, disease model, predictive models, and the methods and metrics used to evaluate the proposed framework.

## 2.1 Data

For this study, we used data on locally acquired dengue cases in Florida, as reported by the US Centers for Disease Control and Prevention (CDC) for the years 2022 and 2023. The two years were combined into a continuous data set that spanned a total of 108 weeks (Figure 1). In Florida, suspected dengue is clinically evaluated and confirmed by laboratory tests. For acute illness (0-7 days after the onset of the symptom), clinicians are advised to order both a nucleic acid amplification test (RT-PCR/NAAT) and an IgM antibody test because the combination detects more cases than either test alone. Specimens are submitted, after coordination with the county health department, to the Florida Department of Health Bureau of Public Health Laboratories (BPHL) or a CLIA-certified commercial laboratory, following Florida Department of Health procedures [76]. Acute serum is shipped refrigerated (2 to 8 ° C) or frozen ( -20 ° C), with acute samples often shipped frozen on dry ice. These standardized testing and reporting requirements strengthen the determination of cases in Florida; consequently, the observed dengue case counts used in this study are likely to be accurate [77–79]. The raw data, number of new cases for each week, can be found in the supplementary file S-Tables-A.

## 2.2 Study location

Florida serves as a practical case study for evaluating our model in a real-world setting of locally acquired dengue. The state spans subtropical to tropical climates on a peninsula bordered by the Gulf of Mexico, the Atlantic Ocean, and the Straits of Florida, with southern counties supporting conditions conducive to year-round arboviral transmission [80]. Although most U.S. dengue cases are travel-associated, sustained local transmission has been documented in Florida, particularly in the south [81], and locally acquired infections have increased in recent years, with more than 60 locally acquired cases reported in 2022 and nearly 200 in 2023 in several counties. This pattern of recurrent and expanding local transmission raises concern that parts of Florida may be on a path toward endemic dengue transmission if current trends continue. At the same time, Florida can still be regarded as a relatively recently affected region, with limited long-term historical data on autochthonous dengue cases. From a modeling standpoint, this combination of emerging endemicity, constrained historical information, and robust surveillance makes Florida a particularly proper setting in which to evaluate and stress-test our DP model, which relies solely on reported human cases.

## 2.3 Disease model

Various compartmental differential equation models with varying levels of detail have been used to capture dengue transmission mechanisms. In this study, we have adopted the two-strain dengue model of Nuraini et al. (2007) to characterize transmission and show that it is possible to advance the ICC-curve method from the basic SIR to the two-population SEIR model of dengue mathematically [82]. The differential equations that govern the model are presented below. The compartments in this model represent different stages of infection status in both human and mosquito populations. Taking a dot to denote the time derivative ( $\frac{dy}{dt} \Rightarrow \dot{y}$ ), the compartments are defined as follows:

$$\begin{aligned}
\dot{S} &= -(B_1 V_1 + B_2 V_2)S - \mu_h S \\
\dot{I}_1 &= B_1 V_1 S - (\gamma + \mu_h) I_1 \\
\dot{R}_1 &= \gamma I_1 - \sigma_2 B_2 V_2 R_1 - \mu_h R_1 \\
\dot{I}_2 &= B_2 V_2 S - (\gamma + \mu_h) I_2 \\
\dot{R}_2 &= \gamma I_2 - \sigma_1 B_1 V_1 R_2 - \mu_h R_2 \\
\dot{D} &= q(\sigma_2 B_2 V_2 R_1 + \sigma_1 B_1 V_1 R_2) - (\mu_h + \gamma) D \\
\dot{Y}_1 &= (1 - q)\sigma_1 B_1 V_1 R_2 - (\gamma + \mu_h) Y_1 \\
\dot{Y}_2 &= (1 - q)\sigma_2 B_2 V_2 R_1 - (\gamma + \mu_h) Y_2 \\
\dot{R} &= \gamma(Y_1 + Y_2 + D) \\
\dot{V}_1 &= A_1(I_1 + Y_1)(1 - V_1 - V_2) - \mu_v V_1 \\
\dot{V}_2 &= A_2(I_2 + Y_2)(1 - V_1 - V_2) - \mu_v V_2
\end{aligned}$$

- $S$ : Human susceptible population (not yet infected by either strain).
- $I_i$ : Infected population with strain  $i$  ( $i = 1, 2$ ).
- $R_i$ : Immune population to strain  $i$  ( $i = 1, 2$ ).
- $Y_i$ : Immune to strain  $j$  ( $j = 2, 1$ ) but infected with strain  $i$  (cross-immunity with active infection).
- $R$ : Population immune to both strains.
- $D$ : Immune to one strain, infected with the other, with severe disease (DHF).
- $V_i$ : Vector population infected by strain  $i$  ( $i = 1, 2$ ).

## 2.4 Predictive model

In this section, we explain the theory and methods we used to advance the ICC curve model from a basic SIR model to a compartmental model for dengue. We also explain how to account for the outbreak season in this model and then introduce the censored Poisson model based on the ICC curve model. Finally, we describe how to establish the Bayesian model grounded in the theory of the ICC curve that counts for error in data reporting and curve fitting process.

### 2.4.1 Predictive ICC-curve method for dengue

Based on the compartmental framework introduced in Section 2.3 and the further detailed mathematical operation in Appendix A, the cumulative number of cases  $C(t)$  for a given outbreak is found to be as follows:

$$\dot{C} \propto C(L_0 - C) \Rightarrow \dot{C} = W C(L_0 - C) = W L_0 C \left(1 - \frac{C}{L_0}\right), \quad (1)$$

where  $L_0$  denotes the final epidemic size and  $W$  represents the intrinsic growth-rate constant. The general form of Equation 1 highlights two key points: first, it represents a differential equation that describes logistic growth over time; and second, the rate of change (number of new cases) is a quadratic function, in the form of an inverted parabola, with respect to the cumulative number of cases. These two important features will provide a method for predicting the number of new cases during a given dengue outbreak.

From a statistical perspective, the result means that the epidemic trajectory can be defined by a logistic growth curve.

$$C_t = \frac{L_0}{1 + \exp\{-\delta(t - \mu)\}}, \quad (2)$$

where  $C_t$  denotes the cumulative number of cases reported at time  $t$ ,  $L_0$  is the final size of the outbreak,  $\mu$  is the mean distribution and  $\delta$  controls the growth rate. The

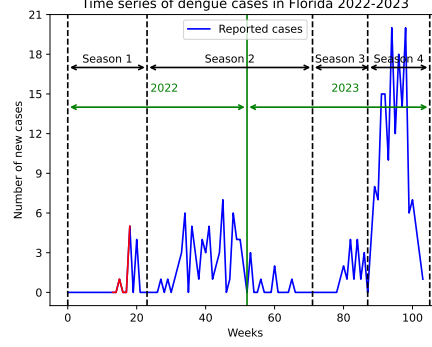


**Fig 1.** Time series of new cases in Florida for 2022-2023, highlighting the outbreak seasons.

cumulative curve (2) can be written as the multiplication of two terms of  $L_0$  and  $\frac{1}{1+\exp\{-\delta(t-\mu)\}}$ . The second part is a cumulative distribution function (CDF) of a logistic random variable ( $T$ ), so  $C_t = L_0 P(T \leq t)$ . Importantly, for a given dengue outbreak, the time to infection  $T$ , the time at which an individual of the final infected population becomes infected, is distributed as a logistic random variable. This formulation offers a probabilistic interpretation of the epidemic curve, where  $\mu$  and  $\delta^{-1}$  represent the location and scale of the underlying logistic distribution.

#### 2.4.2 Outbreak season and ICC-curve method

Before applying this method to real data, it is essential to understand the outbreak season. Vector-borne diseases such as dengue or the West Nile virus typically exhibit seasonal behavior. This means that outbreaks occur during specific periods; outside of this transmission season, disease transmission is minimal or almost non-existent. In some endemic regions, dengue transmission persists throughout the year without a zero-case interval. Consequently, it is essential to establish a precise operational definition of the outbreak season, as this temporal delineation is necessary to apply the ICC curve method to predict case counts.

As discussed in Section 2.4.1, for dengue infection, the time to infection variable which defines the outbreak trajectory follows a logistic probability density function. The logistic probability density function is symmetric around its mean and the cumulative distribution given by  $t_0$  is  $P(T \leq t_0) = \frac{1}{1+\exp(-\delta(t_0-m))}$  (S-Figures-A). This symmetry helps determine the starting point of the outbreak, which is crucial to fitting the model to the data. To identify the starting point, it is essential to analyze historical time-series data. By plotting data for at least one year prior, we can observe when the number of cases reaches its minimum value (also we can check the symmetry), and this minimum value is the end point of an outbreak and starting point of the next one. Practically, an increase in the time series of new cases following several consecutive zero-count time units (e.g., several weeks with zero cases) can be interpreted as the start of a new season. Notably, the emphasis is on 'minimum' rather than 'zero,' as some regions never see dengue cases drop to zero. Such plots provide a clear picture of seasonality and help pinpoint the beginning of the outbreak season. For example, Figure 1 shows the time series of new cases in Florida from 2022 to 2023, and if we consider specifically season 2, it is observed that at the beginning of 2023, the number of cases reflects the tail end of the outbreak that began in 2022. If we aim to predict the outbreak for January 2023, the model must incorporate data from the 2022 outbreak. Similarly, for predictions for August 2023 and beyond, the starting point should be set after the eighth week, as the

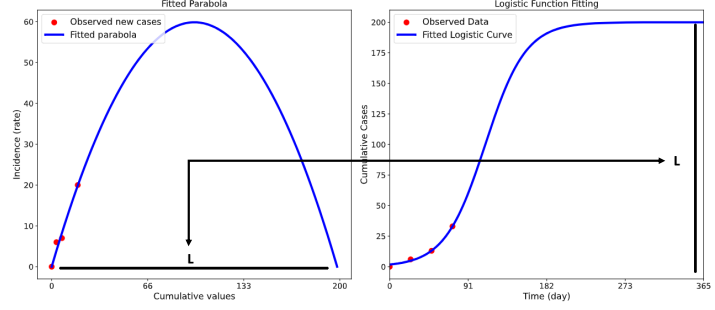


**Fig 2.** Fitted parabola and logistic function to the data at the beginning of the outbreak. As it is seen from parabola,  $L$  is prediction of the final size of the epidemic which has been used to fit the logistic curve of the epidemic trajectory.

second outbreak season in 2023 begins around that time. To accurately predict new cases, the ICC curve must therefore be constructed using data from after the eighth week.

#### 2.4.3 Outbreak prediction using ICC curve method

The method described in Section 2.4.1 explains that the relationship between the cumulative number of cases and the rate of new cases can be represented as a parabola. This structure implies that the final size of the epidemic  $L_0$ , the total number of cases by the end of the outbreak, can be predicted from the domain of this parabola. Specifically, when a sample is available from the beginning of an outbreak, we can fit a parabola to the data (plotting the cumulative cases against the rate of new cases) and thereby obtain a predict of the final epidemic size. Once this final size has been predicted, we then fit a logistic function in the time domain using the predicted final size together with the early-time incidence data. This procedure yields forecasts of the cumulative number of cases at each time point (Figure 2).

As a real example, S-Figures-B shows the point prediction procedure for Florida 2023. Panel (a) shows the data used and panels (b) and (c) shows the fitted parabola and logistic trajectory of the epidemic that can explain the rest of the outbreak in season 2.

For the general forecast process in Florida, we used data from the outbreak onset up to and including week  $t_0$ . Based on the logistic function fitted to this period, we predicted cumulative number of cases for the subsequent four weeks, namely  $t_0 + 1$ ,  $t_0 + 2$ ,  $t_0 + 3$ , and  $t_0 + 4$ . In practice, we modeled the cumulative number of cases for week  $t$  as a left-censored Poisson random variable. The Poisson mean  $C_t$  is given by the ICC curve forecast for week  $t$ , and support is restricted to  $[R_{t-1}, \infty)$ , where  $R_{t-1}$  is the cumulative number of cases reported to  $t - 1$ .

Let  $N_t$  denote the cumulative number of cases for week  $t$ .

We assumed:

$$N_t \sim \text{CPoisson}(C_t, [0, R_{t-1}])$$

in which  $\text{CPoisson}(C_t, [0, R_{t-1}])$  is a Poisson pmf with parameter  $\lambda = C_t$  whose domain

has been censored on  $[0, R_{t-1})$ . Equivalently, the pmf is

$$\Pr(N_t = n) = \begin{cases} \frac{e^{-C_t} C_t^n / n!}{\sum_{k=0}^{R_{t-1}-1} e^{-C_t} \frac{C_t^k}{k!}}, & n \geq R_{t-1}, \\ 0, & n < R_{t-1}. \end{cases} \quad (3)$$

#### 2.4.4 Bayesian approach

Let  $\{X_i\}_{i=1}^p$  denote the weekly number of reported dengue cases in  $p$  weeks of an outbreak. Based on the theory of the ICC curve for dengue, the temporal trajectory of the outbreak is represented by a logistic random variable  $T$ . In practice, however, surveillance data are subject to both under and over reporting, and the final size parameter  $L$  can be misestimated when a parabolic approximation is fitted directly to the observations. To accommodate these imperfections, we embed the reporting error in a Bayesian model, treating it as an observational noise term so that the associated uncertainty is approximated through to the posterior inference.

#### 2.4.5 Trajectory of the outbreak mechanism

As we saw in section 2.4.1, the outbreak trajectory is described by a logistic random variable.

$$\mathbf{T} \sim \text{Logistic}(\mu(\mathbf{O}_p, L), \delta(\mathbf{O}_p, L)), \quad (4)$$

where  $\mathbf{O}_p = (O_1, \dots, O_p)^\top$  and  $L$  are the latent vector of true weekly cases and the final size of the epidemic, respectively. In addition,  $\mu(\mathbf{O}_p, L)$  and  $\delta(\mathbf{O}_p, L)$  are the location and rate parameters obtained from the ICC curve.

#### 2.4.6 Observation model

Each weekly report is modeled as the true incidence perturbed by additive Gaussian measurement error. Denote the number of new cases to week  $p$  by

$$\mathbf{x}_p = (x_1, \dots, x_p)^\top, \quad \mathbf{O}_p = (O_1, \dots, O_p)^\top,$$

where  $\mathbf{O}_p$  is the corresponding latent (error-free) vector.

We assume

$$\mathbf{O}_p = \mathbf{x}_p + \mathbf{e}_p, \quad \mathbf{e}_p \sim \mathcal{N}(\mathbf{0}, \delta_e \mathbf{I}_p) \implies \mathbf{O}_p \mid \mathbf{x}_p \sim \mathcal{N}(\mathbf{x}_p, \delta_e \mathbf{I}_p). \quad (5)$$

Because weekly case numbers are intrinsically nonnegative, we imposed a left-truncated (censored) Gaussian prior on every component of the

$$\mathbf{O}_p \mid \mathbf{x}_p \sim \text{TN}_{[0, \infty)}(\mathbf{x}_p, \delta_e \mathbf{I}_p), \quad (6)$$

where  $\text{TN}_{[0, \infty)}(\mu, \Sigma)$  denotes the multivariate normal distribution  $\mathcal{N}(\mu, \Sigma)$  restricted to the non-negative orthant. This specification guaranties  $O_t \geq 0$  for every week  $t$  while retaining the familiar Gaussian shape within the admissible region. The value of  $\delta_e$  should reflect the context: specifically, the precision of the reporting and diagnostic protocols used. Consequently,  $\delta_e$  will be higher (allowing greater observation noise) in settings where testing is costly or infeasible and case confirmation is based primarily on clinical symptoms, and lower in settings with standardized laboratory confirmation (e.g. NAAT / RT-PCR, NS1, or repeated serology) and rigorous reporting procedures. For this case study, in this setting, we assume that the weekly reported data of new cases

are accurate. This assumption is supported by the rigorous evaluation of suspected dengue patients in Florida and the use of standardized diagnostic protocols for individuals referred to hospitals or public health laboratories [77–79]. Consistent with this high ascertainment, we placed a tight observation prior to the reported counts, specifying a variance of 0.3 for  $\pi(\mathbf{O})$ . This corresponds to a standard deviation of approximately 0.55 cases, which reflects small, but nonzero, week-to-week reporting noise expected under aggregated laboratory-confirmed surveillance. In practical terms, this prior allows draws that fall modestly below or above the reported count while strongly concentrating mass near the observed value, thereby encoding reporting precision without treating counts as error-free.

#### 2.4.7 Model of final size of the epidemic

Using the ICC curve method, we assigned a left-truncated Gaussian prior to the final size parameter  $L$ . The mean of the distribution ( $L_0$ ) is obtained from the ICC curve method to weekly observations  $\{X_i\}_{i=1}^p$ , and the prior variance is denoted by  $\delta_L$ . To ensure that the final size cannot be less than the cumulative number of reported cases  $S = \sum_{i=1}^p X_i$ , the distribution is truncated below at  $S$ :

$$L \sim \mathcal{N}_{[S, \infty)}(L_0, \delta_L), \quad (7)$$

For settings where no prior information on  $\delta_L$  is available, we adopted a very large variance prior for  $L$  that approximates a non-informative prior, which is appropriate when no prior knowledge is imposed.

#### 2.4.8 Posterior distribution

Applying Bayes' theorem with the parameter vector  $\theta = (\mathbf{O}, L)$  yields

$$\begin{aligned} \pi(\theta \mid T = t) &\propto f(T \mid \theta) f(\theta) \\ &= f(T \mid \mathbf{O}, L) f(\mathbf{O}, L) \propto f(T \mid \mathbf{O}, L) f(L \mid \mathbf{O}) \pi(\mathbf{O}). \end{aligned}$$

To facilitate computation, we assumed the prior independence between  $L$  and  $\mathbf{O}$ . Under this assumption, the joint posterior simplifies to

$$\pi(\mathbf{O}, L \mid T = t) \propto f(T \mid \mathbf{O}, L) f(L) \pi(\mathbf{O}).$$

Combining the truncated Gaussian priors (6) and (7) with the logistic likelihood (4) yields the unnormalized posterior density.

$$\begin{aligned} \pi(\mathbf{O}_p, L \mid T = t) &\propto \frac{\delta(\mathbf{O}_p, L) \exp[-\delta(\mathbf{O}_p, L) (t - \mu(\mathbf{O}_p, L))]}{[1 + \exp(-\delta(\mathbf{O}_p, L) (t - \mu(\mathbf{O}_p, L)))]^2} \\ &\times \mathbf{1}_{\{\mathbf{O}_p \geq 0\}} (2\pi\delta_e)^{-p/2} \exp\left[-\frac{1}{2\delta_e} \|\mathbf{O}_p - \mathbf{x}_p\|^2\right] \\ &\times \mathbf{1}_{\{L \geq S\}} (2\pi\delta_L)^{-1/2} \exp\left[-\frac{(L-L_0)^2}{2\delta_L}\right]. \end{aligned} \quad (8)$$

Here,  $\mathbf{1}_{\{\mathbf{O}_p \geq 0\}}$  and  $\mathbf{1}_{\{L \geq S\}}$  enforce the non-negative support. It is important to note that what we have done is essentially to use the information from  $p$  weeks to obtain a posterior as a function of time  $t > p$ . This approach enables us to infer the future trajectory on the basis of the available data.

### 2.4.9 Sampling and prediction

The unnormalized posterior in equation (8) lacks a closed-form normalizing constant; consequently, we employ Markov-chain Monte Carlo (MCMC) to draw samples from the joint distribution  $(\mathbf{O}_p, L) \mid T = t$ . At each iteration, a proposal  $(\mathbf{O}_p^*, L^*)$  is obtained by adding independent Gaussian increments to the current state and reflecting the result in the admissible regions  $\mathbf{O}_p \geq \mathbf{0}$  and  $L \geq S$ . The candidate is accepted with the Metropolis–Hastings probability computed from the posterior kernel in (8); otherwise, the chain retains its previous value. Because every smooth functional of  $(\mathbf{O}_p, L)$  inherits a posterior distribution by transformation of retained draws, no further numerical integration is required. In particular, after each accepted update we apply the ICC-curve procedure to  $(\mathbf{O}_p, L)$  to obtain the logistic parameters  $\mu(\mathbf{O}_p, L)$  and  $\delta(\mathbf{O}_p, L)$ . The predictive cumulative number of cases at time  $t$  is then evaluated as

$$C_t = \frac{L}{1 + \exp\left\{-\delta(\mathbf{O}_p, L)[t - \mu(\mathbf{O}_p, L)]\right\}},$$

yields a posterior sample  $\{C_t\}$  at no additional computational cost. A histogram or kernel density estimate of this sample approximates the predictive density  $\pi(C_t \mid \mathbf{T} = \mathbf{t})$ , providing a fully Bayesian forecast that propagates both epidemiological uncertainty and measurement error. A detailed description of this MCMC algorithm is provided in Appendix B.

## 2.5 Evaluation

In this section, we present the methodologies used to evaluate the results of our work, encompassing point estimation, a Bayesian inference framework, and diagnostics for Markov chain Monte Carlo (MCMC) sampling.

### 2.5.1. Point prediction

To evaluate the performance of the model, we used three complementary approaches to assess its precision. For point prediction, we calculated the root mean square error (RMSE) between point prediction and the real value of cumulative cases reported for each week. As another metric to evaluate the accuracy of the point prediction, the distribution of absolute value of error (AVE) has also been calculated. In addition, we evaluated point predictions using the logarithmic score adopted by CDC in its open prediction challenge for the West Nile virus (WNV) [83]. This method evaluates the point predictions based on their uncertainty, rather than only the single point estimate. If the observed number of cases falls in a region of the probability density function of the point prediction with higher probability, it receives a higher score. Details are provided in Appendix C, and Figure 3 illustrates the evaluation and scoring process.

### 2.5.2. Bayesian approach

For Bayesian point prediction, we have considered the median and mean of the posterior as Bayesian point estimation and based on that calculated  $RMSE_B$ , which is RMSE between Bayesian prediction and the value of real cumulative cases reported for weeks. We also used the logarithmic score for the Bayesian approach.

### 2.5.3. MCMC diagnostics

In addition to evaluating predictive performance, we assessed the quality of the MCMC sampling itself. We ran four independent Metropolis–Hastings chains, each long enough

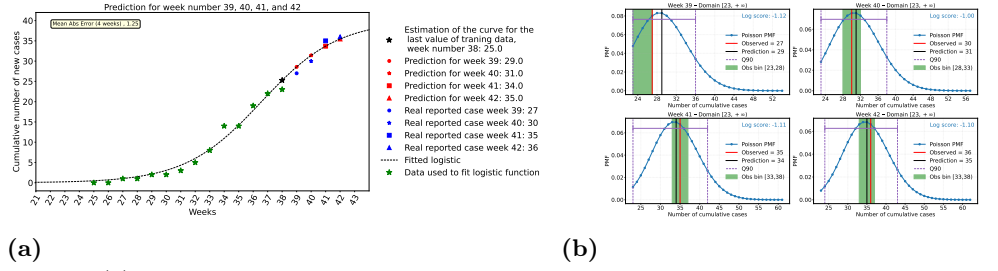


**Fig 3.** (a) Shows the logistic trajectory of the epidemic obtained by ICC-curve method and the values of prediction for four weeks ahead and the real reported cases; (b) Shows the result of the prediction based on the censored Poisson model. The prediction obtained in panel (a) is used as rate for the Poisson model. Also for each week winner epidemiological bins has been shown by orange region

to yield a sufficiently large effective sample size (ESS). For each chain, the first  $1 \times 10^4$  accepted draws were discarded as burn-in to remove transient behavior, and the remaining samples were thinned by retaining every fifth draw to reduce autocorrelation. Convergence and mixing were evaluated using three standard diagnostics: (i) the split Gelman–Rubin statistic,  $\hat{R}$ , to assess between-chain convergence; (ii) Geweke’s early-versus-late  $Z$ -score to detect residual nonstationarity within chains; and (iii) the integrated-autocorrelation-based ESS, reported for each chain individually and for the pooled set of chains.

## 3 Results

In the following sections, we present the identification of outbreak seasons, the results of the ICC model, and the evaluation of its performance. We also summarize the output of the Bayesian model, including the MCMC diagnostic checks and the predictive results.

### 3.1 Outbreak Season

Based on the season definition procedure described in Section 2.4.2, four distinct outbreak periods were considered in Florida between 2022 and 2023. The time series inspection (Figure 1) indicates that the first outbreak occurred between week 13 and week 21. The second outbreak lasted 43 weeks, beginning in week 25 and ending in week 67. The third outbreak spanned 11 weeks, from week 77 to week 87. The final outbreak, which was the most severe in terms of the number of reported cases, began in week 88 and persisted until week 103, with a total duration of 16 weeks. Figure 1 also shows that the calendar year 2023 comprises (i) the waning phase of the second outbreak, which originated in late 2022, and (ii) a third and fourth independent outbreak initiated in 2023. Thus, although 2023 exhibits three distinct periods of case incidence, only the latter two correspond to independent outbreak seasons.

### 3.2 Point prediction

As explained in section 2.1, to demonstrate the method in practice, we collected data on new locally acquired cases in Florida from the Florida Health Department [84] with the aim of predicting new cases for 2022 and 2023. In total, 258 weekly forecasts were generated, comprising 69 one-week ahead predictions, 66 two-week ahead predictions, 63 three-week ahead predictions, and 60 four-week ahead predictions across all outbreaks.

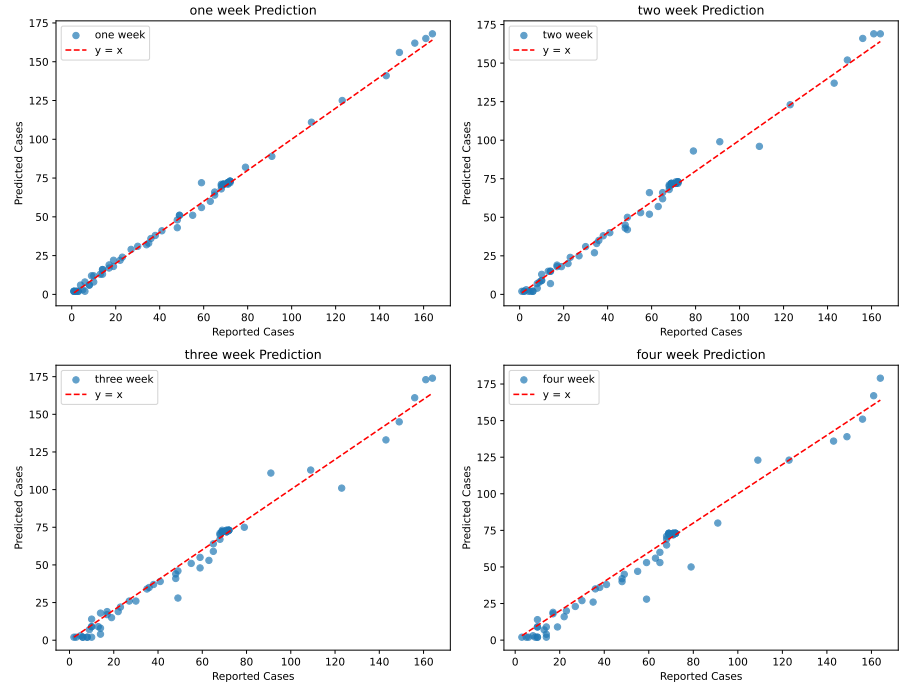


**Fig 4.** One- to four-week ahead predictions of weekly cumulative cases versus reported values in Florida (2022-2023). Each panel corresponds to a forecast horizon (1, 2, 3, or 4 weeks). Reported cases are on the horizontal axis; predicted cases are on the vertical axis. The red dashed line

The distribution of AVE shows that for a one week ahead prediction, 43.48% of the prediction's AVE were less than or equal by one and 78.26% of the prediction's AVE were less than or equal by two cases. More than 95% of the predictions had errors of five cases or fewer, while only less than 4.35% of the predictions have errors greater than or equal to 6. For the forecasts for two weeks ahead, approximately 10.61% of the predictions did not show an error in case counts, while nearly half (43.94%) deviated by at most one case. Errors in two or fewer cases accounted for 59.1% of the predictions, and 80.3% were within five cases. In addition, 16% of the predictions had errors greater than or equal to 6 cases. For the three-week forecasts, exact matches between the predicted and observed cases occurred in 3.2% of the predictions. Deviations in one or two cases represented a little less than half of the results (30.16%). The cumulative accuracy reached 74.6% for errors of up to five cases and exceeded 92% within ten cases. For the four-week ahead forecasts 21% of the predictions, they deviated by only one case. More than half of the forecasts (53.33%) were within four cases. The cumulative accuracy exceeded 93.33% for deviations up to 12 cases. Figure 4 shows the prediction versus real values for the weekly number of cumulative cases. The general RMSE for all outbreaks was 5.7, calculated over 258 weekly predictions encompassing forecast horizons of one, two, three and four-weeks ahead. Across all outbreaks, the RMSE by prediction horizon was 3.81 for one week, 3.57 for two weeks, 2.99 for three weeks and 10.7 for predictions for four-weeks ahead. All results, with additional details, are provided in S-Tables-B.

### 3.2.1 First outbreak

To predict the number of new cases at the beginning of 2022, we used data from the first outbreak, starting from its onset (week 13) until the end of outbreak week 21 of 2022 (Figure 1). In the first step of fitting the parabolic and logistic functions, we considered data from three consecutive weeks, namely weeks 13, 14, and 15, which reported the case 0, 0, and 1, respectively. The predictions were then generated for cumulative cases on horizons of 1, 2, 3, and 4 weeks ahead, corresponding to weeks 16, 17, 18, and 19. In each step, we add one more week to the data for fitting purposes and predicted the next four weeks values. The predicted value for cumulative cases was rounded to the closest integer number (S-Tables-C). All the process of fitting and prediction has been plotted in the supplementary file S-Point-A.

Across outbreak 1, for one-week ahead predictions we observed only three error values (1, 2, and 4): 33.3% of forecasts had an error of exactly one case, 83.3% differed from the observed cases by at most two, and all errors were bounded by four. For two-week ahead predictions, we again observed only three error values (1, 3, and 4): 50.0% of the forecasts had an error of exactly one case, 66.7% were within three cases, and all errors were no greater than four. For three-week ahead predictions, we observed three error values (1, 4, and 8): 33.3% of the forecasts had an error of exactly one case, 83.3% were within four cases, and all errors were bounded by eight. At the four-week ahead horizon, we observed three error values (1, 4, and 8), with 33.3% of forecasts differing from the observed count by only one case, 66.7% within four cases, and all errors were capped at eight (S-Tables-D). For outbreak 1, the RMSE values were 2.24 for the one-week ahead predictions, 2.71 for the two-week-ahead predictions, 4.36 for the three-week ahead predictions, and 5.20 for the four-week-ahead predictions.

### 3.2.2 Second outbreak

For the second outbreak, in the first step we used data from weeks 25, 26, and 27 to forecast weeks 28, 29, 30 and 31, and in each step we added one week to our training data and did 1,2,3, and 4-week ahead prediction as explained before. The predictions results for 1, 2, 3, and 4 weeks ahead have been published in S-Tables-E and all the plots related to Poisson PMF and the fitted parabola and logistic function have been attached to S-Point-A. Across outbreak 2, for one week ahead forecasts, 24.39% of the predictions exactly matched the observed values, while 60.98% deviated by at most one case and 87.8% by no more than two. Errors up to three cases accounted for 95.12% of the forecasts, and all were bounded within five. Two weeks ahead, 15% of the predictions had zero error, more than half (52.5%) were within one case, and approximately three quarters (70%) remained within two. 82.5% of the forecasts had errors less than or equal to three captured and all deviations were limited to seven cases. The three-week horizon showed that 41.03% were within one and 63.85% stayed within two. By three errors, nearly three-quarters (69.23%) were included and all deviations were capped at ten. For the four week prediction, 52.63% of the forecasts had errors of no more than three, 78.95% within six, and all errors were restricted to twelve (S-Tables-F). For outbreak 2, the RMSE values were 1.76 for the predictions made one week in advance, 2.65 for two weeks, 3.73 for three weeks, and 5.31 for four weeks.

### 3.2.3 Third outbreak

For the initial prediction window, we used data from weeks 77, 78, and 79 to forecast weeks 80, 81, 82, and 83. In total, this setup produced 8, 7, 6, and 5 predictions in the one-, two-, three-, and four-week ahead horizons, respectively, and the results are shown in S-Table-G and S-Point-C. For outbreak three, the one-week ahead forecasts showed that 25% of the predictions were exact (error zero), 37.5% were within one case and all

predictions (100%) were within three cases. At two weeks ahead, 57.14.3% of the forecasts had zero error, 100% were within two cases. For the three-week ahead predictions, the absolute error took only four values (0, 2, 4, and 6); 16.7% of the predictions were exact, 50.0% were within two cases and 83.3% were within four cases of the observed counts. For the four-week ahead predictions, the absolute error took five values (1, 2, 5, 6, and 7); none of the predictions were exact, but 40.0% were within two cases, 60.0% were within five cases, 80.0% were within six cases, and all predictions were within seven cases of the observed counts (S-Tables-H). For outbreak three, the RMSE values by prediction horizon were as follows: one-week ahead predictions had an RMSE of 1.80, two-week-ahead predictions 1.51, three-week-ahead predictions 3.55, and four-week-ahead predictions 4.79.

### 3.2.4 Fourth outbreak

The fourth outbreak began in week 87 and continued for 16 weeks. S-Tables-I presents the sets of 14, 13, 12 and 11 weekly forecasts of cumulative case counts, together with the corresponding observations, for the one, two, three and four-week ahead prediction horizons, respectively. In the one-week ahead forecasts, 42.86% of the predictions had an absolute error of 2 cases. Overall, 57.14% of the forecasts were within 3 cases of the observed counts, and approximately 80% were within 5 cases. Detailed results of the distribution of the AVE for the one-, two-, three-, and four-week-ahead predictions are provided in S-Tables-J. The root mean square error (RMSE) for the one-week ahead forecast is  $\text{RMSE} = 5.02$ . For the two-week ahead forecast, the RMSE increases slightly to  $\text{RMSE} = 8.07$ . At three weeks ahead, the RMSE rises more notably to  $\text{RMSE} = 12.62$ , and by four weeks ahead, it reaches  $\text{RMSE} = 15.66$ .

As a summary of the results, all predictions for one, two, three and four-weeks ahead of the cumulative weekly number of cases for all four outbreaks (2022–2023), together with their censored Poisson predictive distributions, are shown in Figure 5. The figure overlays the observed cumulative case counts with the weekly predictive distributions, allowing visual comparison between predicted and observed values across forecast horizons and outbreak periods. All details of these plots and their weekly distributions have been provided in the supplementary file (S-Point).

## 3.3 Bayesian model

### 3.3.1 MCMC diagnostics

To sample from the posterior distribution, we ran four independent MCMC chains. Convergence and mixing were evaluated using standard diagnostics, applied both to the posterior samples of the weekly cumulative number of cases and to the posterior samples of the weekly observations. Figure (6) shows the resulting trace plots together with their corresponding diagnostic statistics for week 86. After discarding burn-in and applying thinning, each chain achieved a sufficiently effective sample size (ESS). The Geweke Z scores satisfied  $|Z| < 2$  for all chains, and the Gelman–Rubin statistic was  $\hat{R} \approx 1.00$  throughout. Visual inspection of the trace plots showed stable behavior with no discernible trends or drifts. All plots have been added to the S-Bayesian.

### 3.3.2 Predictions

During the first outbreak, weeks 16–21, Bayesian point forecasts increased from 3 to 13 cases, with medians that matched the means in all weeks except week 21 (median 12). Mean of absolute errors 2 show a small error for Weekly Bayesian prediction. For the first outbreak, the RMSE is 2.27 for the Bayesian mean forecasts and 2.08 for the Bayesian median forecasts, since the RMSE can be computed separately for each type of

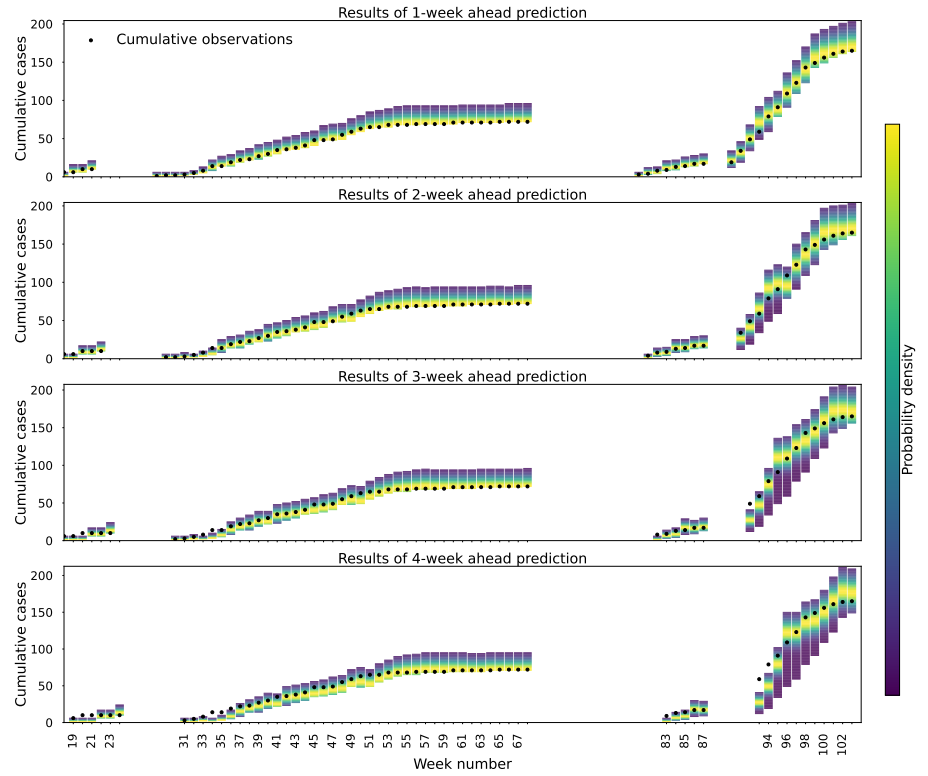


**Fig 5.** Forecasts of cumulative cases by week and their probability densities for four Florida outbreaks (2022–2023) at 1–4-week horizons. Black dots mark observed cases; lighter shading denotes higher probability density.

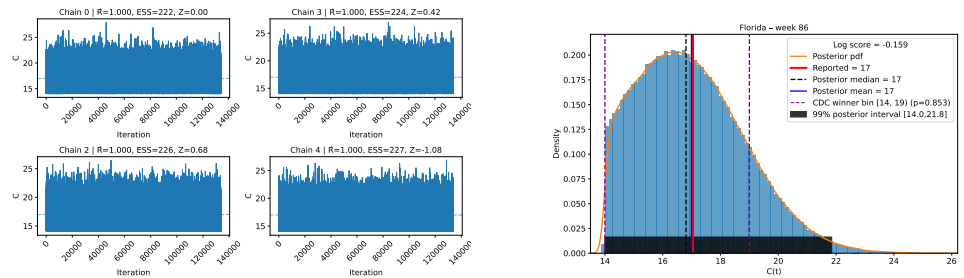


**Fig 6.** (a) shows four MCMC chains of MCMC we have considered for plotting the posterior. (b) shows the posterior PDF, Bayesian predictions, and the real observation for cumulative number of cases for week 86.

point prediction; notably, the RMSE for the Bayesian median (2.08) is smaller than the corresponding value for the censored Poisson model (2.24). The Bayesian model achieved logarithmic scores lower than the censored Poisson model in every week except the first two weeks of the outbreak. All details of prediction, errors, and scores have been provided S-Tables-K and S-Bayesian-A).

During the second outbreak (weeks 29–66), Bayesian point forecasts increased from 3 to 85 cases and generally followed the weekly cumulative reported counts. Absolute error values were small through the middle of the outbreak (mostly 0–3 cases up to week 55) and increased near the late plateau (reaching 12–13 cases by weeks 65–66). The mean absolute error was 3.71 and 3.79 for the posterior mean and median forecasts, respectively, and the RMSE was 5.23 and 5.35 for the Bayesian mean and median. In 23 of the 38 weeks, the Bayesian log scores were closer to zero than the correspondent censored Poisson model (S-Tables-L and S-Bayesian-B).

For the third outbreak, from weeks 80–87, Bayesian point forecasts increased from 3 to 20 cases, while reported cases increased from 3 to 17. The errors were small throughout (0–3 cases), with an exact match in week 86 and near-matches in weeks 80, 81, 84, and 85. The mean absolute error was 1.50 and 1.25 for the posterior mean and median forecasts, respectively, and the corresponding RMSE values were 1.73 and 1.58—both markedly smaller than the corresponding RMSE of 4.36 from the censored Poisson model. Probabilistically, the Bayesian model outperformed the Poisson benchmark in 7 of 8 weeks: its log scores were less negative in weeks 81–87. (S-Tables-M and S-Bayesian-C).

During the fourth outbreak (weeks 90–103), Bayesian point forecasts increased from 22 to 180 cases, with medians closely tracking the means (21 to 180), while reported counts rose from 19 to 165. AVEs ranged from 0 to 15 cases and were generally moderate, with small discrepancies (2–4 cases) in weeks 90, 93, 95, and 100 and an exact match in week 99. Probabilistically, the Bayesian model outperformed the Poisson benchmark in 6 of 14 weeks, mainly during the mid-outbreak period and early plateau (weeks 93, 95 and 99–102), while the Poisson model achieved slightly higher log scores during weeks with sharper incidence changes (e.g., 91–92, 94, 96–98 and 103) (S-Tables-N and S-Bayesian-D). As a visual summary, S-Figures-B display the Bayesian predictive posterior densities for each week alongside the observed data for the four outbreaks during 2022–2023. In addition, Figure 7 shows the Bayesian predictions plotted against the observed counts.

## 4 Discussion

In this study, we developed and evaluated a data parsimonious incidence versus cumulative cases (ICC) curves framework to forecast dengue outbreaks in Florida (2022–2023). Motivated by the limited generalizability and data requirements of many existing forecasting approaches, we extended the ICC model from a basic SIR formulation to a two-population SEIR model of dengue, with only two parameters estimated from human incidence data. We also used an established Bayesian framework based on ICC-curve method to quantify the uncertainty in reported human cases. Our results show that these frameworks reproduce key features of outbreak timing and trajectory with competitive accuracy while requiring only the target year’s case time series as input.

The accurate results and findings (Section 3) suggest that the parsimonious ICC-based model can mitigate some of the generalizability issues seen in location-specific forecasting frameworks. Because the only required input is the time series of new human cases in the target year, the approach does not rely on site-specific mosquito surveillance or detailed environmental covariates. In turn, it eliminates the

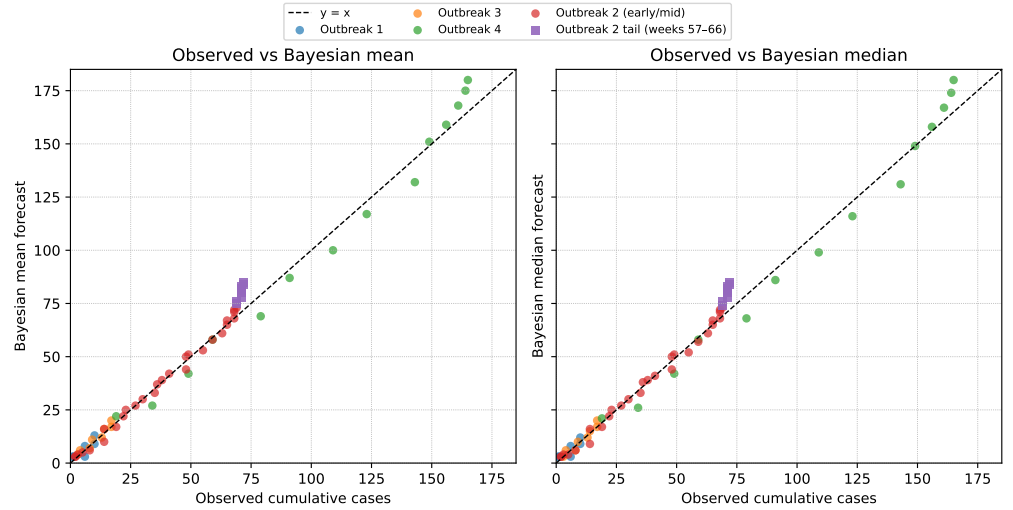


**Fig 7.** Left panel shows predicted versus observed cumulative number of cases for the four outbreaks in 2022–2023 using the Bayesian mean as the point prediction, while the right panel shows the same comparison using the Bayesian median as the point prediction.

need for mosquito-trap data and supports the use of a single model structure across different counties and outbreaks. In addition, by reducing the parameter space to only two epidemiological parameters, the ICC-SEIR extension decreases the noise introduced by high-dimensional parameter estimation and simplifies model calibration. In our Florida application, both the censored Poisson and Bayesian models produced stable forecasts and good predictive accuracy, without requiring heavy model selection or complicated covariate choices. Incorporating observation uncertainty directly into the Bayesian ICC model partially addresses the problem of noisy, under (over) reported incidence. In the Florida application, case reporting is highly accurate and we assumed a small observation variance. As a result, the Bayesian posterior predictive domain intervals, which account for both process and reporting uncertainty, are well calibrated and relatively shorter than the domain of the distributions of censored Poisson model. Finally, because our method does not require a long outbreak history, it remains applicable to locations with limited historical data, which is crucial for newly affected regions or counties where dengue has only recently emerged.

Most locally acquired dengue cases in Florida have occurred in the southern part of the state, particularly in Miami-Dade and, to a lesser extent, Monroe County [85, 86]. To evaluate the ecological plausibility of our risk predictions in the Florida setting, we compared the model-based risk indices, the median of the censored Poisson model for each week prediction, with the weekly abundance of *Aedes aegypti* in Miami-Dade County for the year 2022. Although we only observe a single seasonal cycle and cannot assess whether these patterns are stable across years, the results are nevertheless consistent with field data and with other published studies. Within the single-year time series, lagged Spearman correlations between weekly *Aedes aegypti* abundance and model-predicted dengue risk (1 to 4-weeks ahead) reveal a consistent signal in the 8 to 10-week lag window (Figure 8 and S-Tables-O). An 8–10 week lag between vector dynamics and dengue risk is consistent with previous studies in Mexico, Sri Lanka, and southern Brazil [86–88]. For 1-week ahead predictions, the correlation appears with lags of about 7 to 8 weeks (if  $p\text{-value} \leq 0.1$ ). For the 2- and 3-week ahead predictions, similar patterns are observed with lags of about (7-9) weeks and (8-10), and for the

4-week ahead predictions the strongest correlations occur at lags of approximately 8 to 10 weeks. Together, these results suggest that within this season, the seasonal pattern of mosquito abundance aligns strongly with the temporal pattern of predicted dengue risk at lags of roughly 8-10 weeks.

These lagged relationships and the accurate predictive performance of the model (quantified in Section 3) may point to two possible implications for mitigation strategies. First, the estimated 8-10 week delay between *Aedes aegypti* abundance and dengue risk with the 1,2,3 and 4-weeks ahead implies an effective lead time on the order of approximately 2 months between elevated mosquito abundance and subsequent increases in human risk. In the Florida time series 2022-2023 (Figure 1), this suggests two main windows for intensified adulticiding for 2022: one early in the calendar year, preceding the initial increase in cases, and a second period beginning shortly after week 20, ahead of the larger late-season outbreak. Second, the correlation between mosquito abundance and the 4-week ahead predictions indicates that an operational threshold on the 4-week ahead forecast could be used to trigger targeted adulticiding, with approximately one month available to reduce adult mosquito abundance before the anticipated increase in transmission. Although these analyses highlight a clear correlation between mosquito abundance and predicted dengue risk, they are based on a single year of data. More precise estimates of the underlying ecological lag would require multi-year entomological surveillance and case data, which are currently limited for this setting.

Although detailed and time-resolved information on mosquito management in Miami-Dade is not available, the Florida Department of Health issued mosquito-borne dengue illness alerts in weeks 29–33 of 2022. Probably, adulticiding was initiated or intensified during this advisory period and contributed to reducing both risk and incident cases. Hence, the cases reported after this window can be interpreted as occurring under enhanced control. Under this assumption, the number of cases that might have occurred in the absence of such a program could plausibly lie closer to the upper quintile (for example, the 75th percentile) of the weekly risk distribution, as indicated by the blue circles in Figure 8.

Beyond these implications for timing and control, the Bayesian framework also affects how we interpret uncertainty in forecasts. Although the Bayesian model was primarily designed to account for reporting error rather than to replace the Poisson model, in most weeks its predictions are actually more precise: the posterior predictive intervals are shorter than the corresponding intervals from the censored Poisson model. This is mainly because we assumed a very small variance for the observation error. In other words, based on the testing procedures and protocols for patient diagnosis and protocols used by the CDC and Florida Department of Health explained in Section 2.4.6, we specified a small reporting error, and this choice is directly reflected in the narrow posterior predictive intervals.

In addition, the Bayesian model provides evidence supporting the high precision of dengue case reporting by the Florida Department of Health. We examined the posterior distribution of the true observations given the weekly reported counts,  $\pi(O_p | \mathbf{x})$ , and found that for each week, the posterior mean (median) was equal to or slightly greater than the corresponding reported case count, reflecting the small observation-error variance specified in Section 2.4.6 (for example S-Bayesian-E). The posterior that gives more density to the regions greater than the reported cases for each week is plausibly interpreted as capturing unobserved infections, such as asymptomatic cases or patients who did not seek care. By contrast, a posterior with insisting on the regions falling below the reported counts would be difficult to reconcile with the high diagnostic specificity of Florida’s dengue surveillance, where false-positive case confirmations are expected to be rare. Another noteworthy feature of the Bayesian framework appears near the end of outbreak 2: the Bayesian model extends the tail of the epidemic further

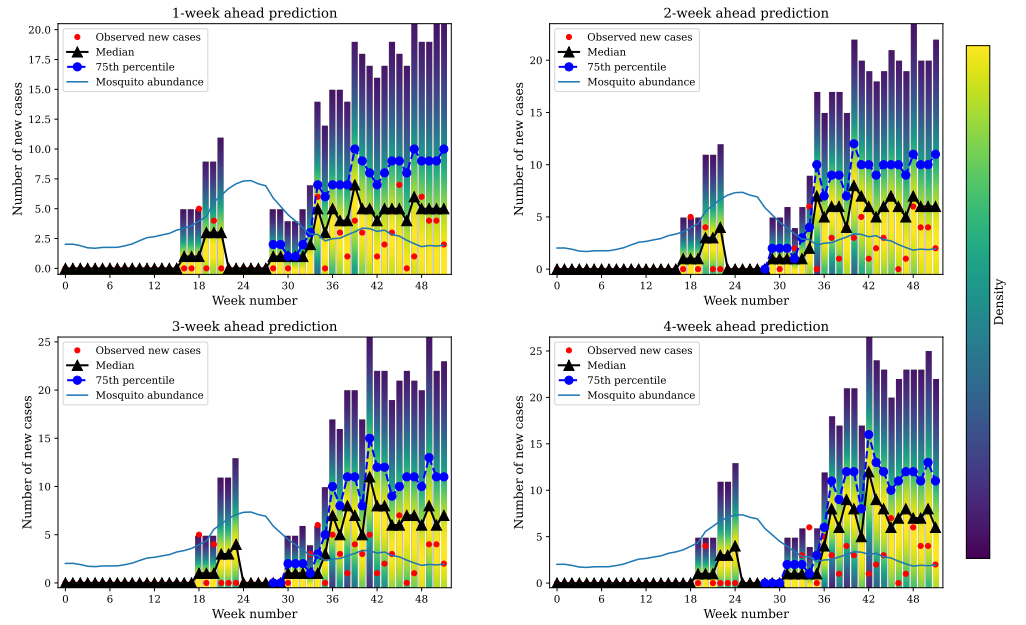


**Fig 8.** Each panel shows the censored Poisson model for the corresponding weekly prediction. The point prediction of risk for each week is shown by black triangles, representing the median of the censored Poisson distribution. Observed reported case counts are shown by red dots, and the blue curve depicts the smoothed weekly abundance of mosquitoes in traps.

in time than the censored Poisson model. This behavior of the weekly posterior is consistent with isolated weeks with nonzero reported cases after weeks 56, 60, and 65, and may indicate additional symptomatic infections that were not captured in other weeks or performing a mosquito control program (S-Figures-C).

Despite these encouraging results, the proposed modeling framework has several limitations that warrant consideration. First, the model is entirely based on the reported incidence, which is known to underestimate true dengue infections due to mild and asymptomatic cases. Although the Bayesian framework partially accommodates reporting uncertainty, we do not explicitly model under reporting mechanisms, and therefore our forecasts reflect only the dynamics of detected cases. Second, by design, this model operates only after human cases begin to be reported. This limitation can be addressed by using historical case time series to predict the onset of the outbreak before reporting begins. Third, our evaluation is restricted to outbreaks in Florida between 2022 and 2023; future work should assess how well the ICC-based approach generalizes to other regions and to longer time horizons.

## Acknowledgments

This work has been supported by the USDA National Institute of Food and Agriculture, grant number 2022-67015-38059 through the NSF/NIH/USDA/BBSRC/BSF/NSFC Ecology and Evolution of Infectious Diseases Program, and the United States Department of Agriculture ARS under agreements number 58-3022-1-010 and 58-3022-3-025.

# CRedit authorship contribution statement

**Saman Hosseini:** Conceptualization, data curation, formal analysis, investigation, methodology, validation, visualization, writing original draft, writing review editing.

**Lee W. Cohnstaedt:** Conceptualization, methodology, resources, supervision, validation, writing original draft, writing, review editing.

**Caterina Scoglio:** Conceptualization, formal analysis, funding acquisition, methodology, project administration, supervision, validation, writing original draft, writing, review editing.

## References

1. Simmons CP, Farrar JJ, van Vinh Chau N, Wills B. Dengue. *New England Journal of Medicine*. 2012;366(15):1423-32.
2. Ross TM. Dengue virus. *Clinics in laboratory medicine*. 2010;30(1):149.
3. Schaffner F, Mathis A. Dengue and dengue vectors in the WHO European region: past, present, and scenarios for the future. *The Lancet Infectious Diseases*. 2014;14(12):1271-80.
4. Organization WH. Dengue and severe dengue. World Health Organization; 2025. Accessed 21 October 2025. Available from: <https://www.who.int/news-room/fact-sheets/detail/dengue-and-severe-dengue>.
5. Paixão ES, Costa MdCN, Rodrigues LC, Rasella D, Cardim LL, Brasileiro AC, et al. Trends and factors associated with dengue mortality and fatality in Brazil. *Revista da Sociedade Brasileira de Medicina Tropical*. 2015;48(4):399-405.
6. Lai JH, Lin YL, Hsieh SL. Pharmacological intervention for dengue virus infection. *Biochemical Pharmacology*. 2017;129:14-25.
7. Thomas SJ. Is new dengue vaccine efficacy data a relief or cause for concern? *npj Vaccines*. 2023;8(1):55.
8. Knerer G, Currie CS, Brailsford SC. Impact of combined vector-control and vaccination strategies on transmission dynamics of dengue fever: a model-based analysis. *Health care management science*. 2015;18(2):205-17.
9. Rather IA, Parray HA, Lone JB, Paek WK, Lim J, Bajpai VK, et al. Prevention and control strategies to counter dengue virus infection. *Frontiers in cellular and infection microbiology*. 2017;7:336.
10. Ranathunge T, Harishchandra J, Maiga H, Bouyer J, Gunawardena YNS, Hapugoda M. Development of the Sterile Insect Technique to control the dengue vector *Aedes aegypti* (Linnaeus) in Sri Lanka. *Plos one*. 2022;17(4):e0265244.
11. Bowman LR, Runge-Ranzinger S, McCall PJ. Assessing the relationship between vector indices and dengue transmission: a systematic review of the evidence. *PLoS neglected tropical diseases*. 2014;8(5):e2848.
12. Sasmita HI, Neoh KB, Yusmalinar S, Anggraeni T, Chang NT, Bong LJ, et al. Ovitrap surveillance of dengue vector mosquitoes in Bandung city, West Java province, Indonesia. *PLoS neglected tropical diseases*. 2021;15(10):e0009896.
13. Ong J, Aik J, Ng LC. Adult *Aedes* abundance and risk of dengue transmission. *PLoS Neglected Tropical Diseases*. 2021;15(6):e0009475.

14. Lega J, Brown HE, Barrera R. *Aedes aegypti* (Diptera: Culicidae) abundance model improved with relative humidity and precipitation-driven egg hatching. *Journal of medical entomology*. 2017;54(5):1375-84.
15. Tran A, L'ambert G, Lacour G, Benoît R, Demarchi M, Cros M, et al. A rainfall-and temperature-driven abundance model for *Aedes albopictus* populations. *International journal of environmental research and public health*. 2013;10(5):1698-719.
16. Serpa LLN, Monteiro Marques GRA, de Lima AP, Voltolini JC, Arduino MdB, Barbosa GL, et al. Study of the distribution and abundance of the eggs of *Aedes aegypti* and *Aedes albopictus* according to the habitat and meteorological variables, municipality of São Sebastião, São Paulo State, Brazil. *Parasites & Vectors*. 2013;6(1):321.
17. Wang F, Zhu Y, Zhang H, Fan J, Leng P, Zhou J, et al. Spatial and temporal analyses of the influences of meteorological and environmental factors on *Aedes albopictus* (Diptera: Culicidae) population dynamics during the peak abundance period at a city scale. *Acta Tropica*. 2023;245:106964.
18. Siritiasatien P, Chadsuthi S, Jampachaisri K, Kesorn K. Dengue epidemics prediction: A survey of the state-of-the-art based on data science processes. *IEEE Access*. 2018;6:53757-95.
19. Buczak AL, Koshute PT, Babin SM, Feighner BH, Lewis SH. A data-driven epidemiological prediction method for dengue outbreaks using local and remote sensing data. *BMC medical informatics and decision making*. 2012;12(1):124.
20. Naish S, Dale P, Mackenzie JS, McBride J, Mengersen K, Tong S. Climate change and dengue: a critical and systematic review of quantitative modelling approaches. *BMC infectious diseases*. 2014;14(1):167.
21. Gharbi M, Quenel P, Gustave J, Cassadou S, Ruche GL, Girdary L, et al. Time series analysis of dengue incidence in Guadeloupe, French West Indies: forecasting models using climate variables as predictors. *BMC infectious diseases*. 2011;11(1):166.
22. McLennan-Smith TA, Mercer GN. Complex behaviour in a dengue model with a seasonally varying vector population. *Mathematical biosciences*. 2014;248:22-30.
23. Karim MN, Munshi SU, Anwar N, Alam MS. Climatic factors influencing dengue cases in Dhaka city: a model for dengue prediction. *Indian journal of medical research*. 2012;136(1):32-9.
24. Wu PC, Lay JG, Guo HR, Lin CY, Lung SC, Su HJ. Higher temperature and urbanization affect the spatial patterns of dengue fever transmission in subtropical Taiwan. *Science of the total Environment*. 2009;407(7):2224-33.
25. Reiter P, Lathrop S, Bunning M, Biggerstaff B, Singer D, Tiwari T, et al. Texas lifestyle limits transmission of dengue virus. *Emerging infectious diseases*. 2003;9(1):86.
26. Wongkoon S, Jaroensutasinee M, Jaroensutasinee K. Weather factors influencing the occurrence of dengue fever in Nakhon Si Thammarat, Thailand. *Tropical Biomedicine*. 2013.

27. Xu HY, Fu X, Lee LKH, Ma S, Goh KT, Wong J, et al. Statistical modeling reveals the effect of absolute humidity on dengue in Singapore. *PLoS neglected tropical diseases*. 2014;8(5):e2805.
28. Machado-Machado EA. Empirical mapping of suitability to dengue fever in Mexico using species distribution modeling. *Applied Geography*. 2012;33:82-93.
29. Runge-Ranzinger S, Horstick O, Marx M, Kroeger A. What does dengue disease surveillance contribute to predicting and detecting outbreaks and describing trends? *Tropical Medicine & International Health*. 2008;13(8):1022-41.
30. Focks DA, Chadee DD. Pupal survey: an epidemiologically significant surveillance method for *Aedes aegypti*: an example using data from Trinidad. *The American journal of tropical medicine and hygiene*. 1997;56(2):159-67.
31. Seng CM, Setha T, Nealon J, Socheat D. Pupal sampling for *Aedes aegypti* (L.) surveillance and potential stratification of dengue high-risk areas in Cambodia. *Tropical Medicine & International Health*. 2009;14(10):1233-40.
32. Pham HV, Doan HT, Phan TT, Tran Minh NN. Ecological factors associated with dengue fever in a Central Highlands province, Vietnam. *BMC infectious diseases*. 2011;11(1):172.
33. Aburas HM. ABURAS index: A statistically developed index for dengue-transmitting vector population prediction. In: *Proceedings of world academy of science, engineering and technology*. vol. 23; 2007. p. 151-4.
34. Strickman D, Kittayapong P. Dengue and its vectors in Thailand: calculated transmission risk from total pupal counts of *Aedes aegypti* and association of wing-length measurements with aspects of the larval habitat. *The American Journal of Tropical Medicine and Hygiene*. 2003;68(2):209-17.
35. Thongrunkiat S, Wasinpiyamongkol L, Maneekan P, Prummongkol S, Samung Y. Natural transovarial dengue virus infection rate in both sexes of dark and pale forms of *Aedes aegypti* from an urban area of Bangkok, Thailand. *Southeast Asian Journal of Tropical Medicine & Public Health*. 2012;43(5):1146-52.
36. Ponlawat A, Harrington LC. Age and body size influence male sperm capacity of the dengue vector *Aedes aegypti* (Diptera: Culicidae). *Journal of medical entomology*. 2007;44(3):422-6.
37. Limkittikul K, Brett J, L'Azou M. Epidemiological trends of dengue disease in Thailand (2000–2011): a systematic literature review. *PLoS neglected tropical diseases*. 2014;8(11):e3241.
38. Chompoosri J, Thavara U, Tawatsin A, Anantapreecha S, Siriyasatien P. Seasonal monitoring of dengue infection in *Aedes aegypti* and serological feature of patients with suspected dengue in 4 central provinces of Thailand. *The Thai Journal of Veterinary Medicine*. 2012;42(2):185-93.
39. Thavara U, Bhakdeenuan P, Thawatsin A, Chompoosri J, Khumsawads C, Phusup Y, et al. Biology of dengue vectors and serotypes of dengue virus in infectious cycle in Thailand. *Bull Dept Med Sci*. 2015;57(2):186-96.
40. CDC. Dengue hemorrhagic fever–US-Mexico border, 2005. *MMWR Morb Mortal Wkly Rep*. 2007;56:785-9.

41. Knowlton K, Solomon G, Rotkin-Ellman M, Council N. Fever pitch: Mosquito-borne dengue fever threat spreading in the Americas. New York: Natural Resources Defense Council. 2009.
42. Rund SS, Moise IK, Beier JC, Martinez ME. Rescuing troves of hidden ecological data to tackle emerging mosquito-borne diseases. *Journal of the American Mosquito Control Association*. 2019;35(1):75-83.
43. Biswas DK, Bhunia R, Basu M. Dengue fever in a rural area of West Bengal, India, 2012: an outbreak investigation. *WHO South-East Asia Journal of Public Health*. 2014;3(1):46-50.
44. Yu HL, Angulo JM, Cheng MH, Wu J, Christakos G. An online spatiotemporal prediction model for dengue fever epidemic in Kaohsiung (Taiwan). *Biometrical Journal*. 2014;56(3):428-40.
45. C Costa AC, Codeço CT, Honório NA, Pereira GR, N Pinheiro CF, Nobre AA. Surveillance of dengue vectors using spatio-temporal Bayesian modeling. *BMC medical informatics and decision making*. 2015;15(1):93.
46. Thiruchelvam L, Dass SC, Zaki R, Yahya A, Asirvadam VS, et al. Correlation analysis of air pollutant index levels and dengue cases across five different zones in Selangor, Malaysia. *Geospatial health*. 2018;13(1).
47. Beatty M, Vorndam V, Hunsperger E, Muñoz J, Clark G. Travel-Associated Dengue Infections—United States, 2001-2004. *MMWR: Morbidity & Mortality Weekly Report*. 2005;54(22).
48. Baaten GG, Sonder GJ, Zaaijer HL, van Gool T, Kint JA, van den Hoek A. Travel-related dengue virus infection, the Netherlands, 2006–2007. *Emerging infectious diseases*. 2011;17(5):821.
49. Ratnam I, Leder K, Black J, Torresi J. Dengue fever and international travel. *Journal of travel medicine*. 2013;20(6):384-93.
50. Hanna JN, Ritchie SA, Richards AR, Taylor CT, Pyke AT, Montgomery BL, et al. Multiple outbreaks of dengue serotype 2 in north Queensland, 2003/04. *Australian and New Zealand journal of public health*. 2006;30(3):220-5.
51. Teichmann D, Göbels K, Niedrig M, Grobusch MP. Dengue virus infection in travellers returning to Berlin, Germany: clinical, laboratory, and diagnostic aspects. *Acta Tropica*. 2004;90(1):87-95.
52. Reiner Jr RC, Stoddard ST, Scott TW. Socially structured human movement shapes dengue transmission despite the diffusive effect of mosquito dispersal. *Epidemics*. 2014;6:30-6.
53. Gardner LM, Fajardo D, Waller ST, Wang O, Sarkar S. A predictive spatial model to quantify the risk of air-travel-associated dengue importation into the United States and Europe. *Journal of tropical medicine*. 2012;2012(1):103679.
54. Hii YL, Zhu H, Ng N, Ng LC, Rocklöv J. Forecast of dengue incidence using temperature and rainfall. *PLoS neglected tropical diseases*. 2012;6(11):e1908.
55. Descloux E, Mangeas M, Menkes CE, Lengaigne M, Leroy A, Tehei T, et al. Climate-based models for understanding and forecasting dengue epidemics. *PLoS neglected tropical diseases*. 2012;6(2):e1470.

56. Lowe R, Barcellos C, Coelho CA, Bailey TC, Coelho GE, Graham R, et al. Dengue outlook for the World Cup in Brazil: an early warning model framework driven by real-time seasonal climate forecasts. *The Lancet infectious diseases*. 2014;14(7):619-26.
57. Ranstam J, Cook JA. LASSO regression. *Journal of British Surgery*. 2018;105(10):1348-8.
58. Shi Y, Liu X, Kok SY, Rajarethinam J, Liang S, Yap G, et al. Three-month real-time dengue forecast models: an early warning system for outbreak alerts and policy decision support in Singapore. *Environmental health perspectives*. 2016;124(9):1369-75.
59. Lowe R, Coelho CA, Barcellos C, Carvalho MS, Catao RDC, Coelho GE, et al. Evaluating probabilistic dengue risk forecasts from a prototype early warning system for Brazil. *Elife*. 2016;5:e11285.
60. Hussain-Alkhateeb L, Kroeger A, Oliaro P, Rocklöv J, Sewe MO, Tejeda G, et al. Early warning and response system (EWARS) for dengue outbreaks: Recent advancements towards widespread applications in critical settings. *PloS one*. 2018;13(5):e0196811.
61. Aburas HM, Cetiner BG, Sari M. Dengue confirmed-cases prediction: A neural network model. *Expert Systems with Applications*. 2010;37(6):4256-60.
62. Adde A, Roucou P, Mangeas M, Ardillon V, Desenclos JC, Rousset D, et al. Predicting dengue fever outbreaks in French Guiana using climate indicators. *PLoS neglected tropical diseases*. 2016;10(4):e0004681.
63. Mazhar B, Ali NM, Manzoor F, Khan MK, Nasir M, Ramzan M. Development of data-driven machine learning models and their potential role in predicting dengue outbreak. *Journal of Vector Borne Diseases*. 2024;61(4):503-14.
64. Edussuriya C, Deegalla S, Gawarammana I. An accurate mathematical model predicting number of dengue cases in tropics. *PLoS neglected tropical diseases*. 2021;15(11):e0009756.
65. Buczak AL, Baugher B, Moniz LJ, Bagley T, Babin SM, Guven E. Ensemble method for dengue prediction. *PloS one*. 2018;13(1):e0189988.
66. Siriyasatien P, Phumee A, Ongruk P, Jampachaisri K, Kesorn K. Analysis of significant factors for dengue fever incidence prediction. *BMC bioinformatics*. 2016;17(1):166.
67. Salim NAM, Wah YB, Reeves C, Smith M, Yaacob WFW, Mudin RN, et al. Prediction of dengue outbreak in Selangor Malaysia using machine learning techniques. *Scientific reports*. 2021;11(1):939.
68. Deb S, Acebedo CML, Dhanapal G, Heng CMC. An ensemble prediction approach to weekly Dengue cases forecasting based on climatic and terrain conditions. *Journal of Health and Social Sciences*. 2017;2(3):257-72.
69. Majeed MA, Shafri HZ, Wayayok A, Zulkaffi Z, et al. Prediction of dengue cases using the attention-based long short-term memory (LSTM) approach. *Geospatial health*. 2023;18(1).

70. Ramadona AL, Lazuardi L, Hii YL, Holmner Å, Kusnanto H, Rocklöv J. Prediction of dengue outbreaks based on disease surveillance and meteorological data. *PloS one*. 2016;11(3):e0152688.
71. Althouse BM, Ng YY, Cummings DA. Prediction of dengue incidence using search query surveillance. *PLoS neglected tropical diseases*. 2011;5(8):e1258.
72. Bal S, Sodoudi S. Modeling and prediction of dengue occurrences in Kolkata, India, based on climate factors. *International journal of biometeorology*. 2020;64(8):1379-91.
73. Chen Y, Ong JHY, Rajarethinam J, Yap G, Ng LC, Cook AR. Neighbourhood level real-time forecasting of dengue cases in tropical urban Singapore. *BMC medicine*. 2018;16(1):129.
74. Lega J, Brown HE. Data-driven outbreak forecasting with a simple nonlinear growth model. *Epidemics*. 2016;17:19-26.
75. Lega J. Parameter estimation from ICC curves. *Journal of biological dynamics*. 2021;15(1):195-212.
76. U S Food and Drug Administration. Clinical Laboratory Improvement Amendments (CLIA); 2023. Accessed November 22, 2025. <https://www.fda.gov/medical-devices/ivd-regulatory-assistance/clinical-laboratory-improvement-amendments-clia>.
77. of Health FD. Dengue virus (DENV) Typing, PCR [Test Menu];. Test code 1681; DH 1847 requisition; store 2–8°C or  $\leq -20^{\circ}\text{C}$ ; ship on dry ice. Available from: [https://www.floridahealth.gov/programs-and-services/public-health-laboratories/\\_documents/\\_test\\_menu/\\_documents/denv\\_pcr.pdf](https://www.floridahealth.gov/programs-and-services/public-health-laboratories/_documents/_test_menu/_documents/denv_pcr.pdf).
78. for Disease Control C, Prevention. Molecular Tests for Dengue Virus; 2025. Guidance on NAAT/RT-PCR use for acute dengue diagnosis. Available from: <https://www.cdc.gov/dengue/hcp/diagnosis-testing/molecular-tests-for-dengue-virus.html>.
79. for Disease Control C, Prevention. Clinical Testing Guidance for Dengue; 2025. Guidance for clinicians on NAAT/RT-PCR, NS1, and IgM testing by illness day. Available from: <https://www.cdc.gov/dengue/hcp/diagnosis-testing/index.html>.
80. Wilke AB, Vasquez C, Medina J, Carvajal A, Petrie W, Beier JC. Community composition and year-round abundance of vector species of mosquitoes make Miami-Dade County, Florida a receptive gateway for arbovirus entry to the United States. *Scientific reports*. 2019;9(1):8732.
81. Stephenson CJ, Coatsworth H, Waits CM, Nazario-Maldonado NM, Mathias DK, Dinglasan RR, et al. Geographic partitioning of dengue virus transmission risk in Florida. *Viruses*. 2021;13(11):2232.
82. Nuraini, Soewono E, Sidarto KA. Mathematical Model of Dengue Disease Transmission with Severe DHF Compartment. *Bulletin of the Malaysian Mathematical Sciences Society*. 2007;30:123-34.
83. Holcomb KM, Mathis S, Staples JE, Fischer M, Barker CM, Beard CB, et al. Evaluation of an open forecasting challenge to assess skill of West Nile virus neuroinvasive disease prediction. *Parasites & Vectors*. 2023;16(1):11.

84. of Health FD. Mosquito-Borne Diseases Surveillance. Florida Department of Health; 2023. [Last Modified Date: Aug 13, 2024 11:47:57 AM]. <https://www.floridahealth.gov/diseases-and-conditions/mosquito-borne-diseases/surveillance.html>.
85. Rey JR. Dengue in Florida (USA). *Insects*. 2014;5(4):991-1000.
86. Eisen L, García-Rejón JE, Gómez-Carro S, Vázquez MDRN, Keefe TJ, Beaty BJ, et al. Temporal correlations between mosquito-based dengue virus surveillance measures or indoor mosquito abundance and dengue case numbers in Merida City, Mexico. *Journal of medical entomology*. 2014;51(4):885-90.
87. Liyanage P, Tozan Y, Tissera HA, Overgaard HJ, Rocklöv J. Assessing the associations between Aedes larval indices and dengue risk in Kalutara district, Sri Lanka: a hierarchical time series analysis from 2010 to 2019. *Parasites & vectors*. 2022;15(1):277.
88. da Cruz Ferreira DA, Degener CM, de Almeida Marques-Toledo C, Bendati MM, Fetzer LO, Teixeira CP, et al. Meteorological variables and mosquito monitoring are good predictors for infestation trends of Aedes aegypti, the vector of dengue, chikungunya and Zika. *Parasites & vectors*. 2017;10(1):78.